Entropy Generation of Williamson Nanofluid near a Stagnation Point over a Moving Plate with Binary Chemical Reaction and Activation Energy

A. Zaib,[1,]* S. Abelman,[2] A.J. Chamkha,[3] & M.M. Rashidi[4]

[1]Department of Mathematical Sciences, Federal Urdu University of Arts, Science & Technology, Gulshan-e-Iqbal Karachi-75300, Pakistan

[2]DST-NRF Centre of Excellence in Mathematical and Statistical Sciences, School of Computer Science and Applied Mathematics, University of the Witwatersrand, Johannesburg, Private Bag 3, Wits 2050, Johannesburg, South Africa

[3]Mechanical Engineering Department, Prince Mohammad Bin Fahd University, Al-Khobar 31952, Saudi Arabia

4Department of Civil Engineering, School of Engineering, University of Birmingham, Birmingham, UK

*Address all correspondence to: A. Zaib, Department of Mathematical Sciences, Federal Urdu University of Arts, Science & Technology, Gulshan-e-Iqbal Karachi-75300, Pakistan, E-mail: zaib20042002@yahoo.com

ABSTRACT: This research explores the impact of entropy generation on stagnation point flow of a non-Newtonian Williamson nanofluid over a moving plate with activation energy and binary chemical reaction. For energy activation a modified Arrhenius function is invoked. Suitable transformation variables are used to simplify the governing flow problem to obtain the self similar solutions. Numerical solutions for temperature distribution, velocity of fluid, concentration of nanoparticle and entropy profile are established and examined using shooting method. Results reveal that the velocity profile reduces due to increasing Williamson parameter, whereas the temperature distribution and concentration of nanoparticle enhance with larger values of Williamson parameter. It is also inspected that the concentration boundary layer increases due to activation energy and decreases due to reaction rate and temperature differences. Moreover, the entropy generation profile is higher for non-Newtonian fluid compared to Newtonian fluid. The results obtained from the present methodology validates when compared with articles in the existing literature. It gives an excellent agreement with the predecessors. The expression for Nusselt and Sherwood numbers are also taken into consideration and presented via graphs and tables.

KEY WORDS: Williamson nanofluid, entropy generation, binary chemical reaction and activation energy, moving plate

NOMENCLATURE

$\tilde{A}_1$	First Rivilin-Erickson tensor
Br	Brinkman number
c	positive constant
C_f	skin friction coefficient
C	concentration of nanoparticle
C_w	concentration of nanoparticle at the surface
C_∞	ambient concentration of nanoparticle
D_B	coefficient of Brownian diffusion [$m^{-2}s^{-1}$]
D_T	coefficient of thermophoresis diffusion [$m^{-2}s^{-1}$]
E_a	activation energy
E	dimensionless activation energy
f	dimensionless stream function

k	thermal conductivity [$Wm^{-1} K$]
k_r^2	chemical reaction rate constant
k^*	mean absorption coefficient
L	characteristic length
m_w	mass flux
I	Identity vector
n	fitted rate constant
Ω	dimensionless temperature difference
ς	dimensionless concentration difference
Nb	Brownian motion parameter
N_G	entropy generation
Nt	thermophoresis parameter
Nu_x	Nusselt number
$\Pr$	Prandtl number
q_w	heat flux [Wm^{-2}]
Re_x	local Reynolds number on the length
Re_L	Reynolds number
Sc	Schmidt number
Sh_x	Sherwood number
$S_{gen}^{'''}$	rate of actual entropy generation
$S_0^{'''}$	rate of characteristic entropy generation
T	temperature [K]

T_∞ free stream temperature [K]

T_w fluid temperature at wall [K]

u_e free stream velocity [ms^{-1}]

u, v velocity components [ms^{-1}]

x, y Cartesian coordinates [m]

X time constant

Greek symbols

α thermal diffusivity [$m^2\ s^{-1}$]

β dimensionless reaction rate

δ temperature difference parameter

γ Williamson fluid parameter

κ Boltzmann constant

λ diffusive constant parameter

$\tilde{\mu}_0, \tilde{\mu}_\infty$ limiting viscosities at zero and infinite shear stresses

π Second invariant strain tensor

ϕ dimensionless concentration of nanoparticle

θ dimensionless temperature

ν kinematic viscosity [m^2s^{-1}]

ρ density [kgm^{-3}]

$(\rho c)_f$ heat capacity of the fluid [$Jm^{-3}K^{-1}$]

$(\rho c)_p$ effective heat capacity of the nanoparticle material [$Jm^{-3}K^{-1}$]

Λ nanoparticle to base fluid heat capacity ratio

Φ	extra stress tensor
τ_w	shear stress at plate [Nm^{-2}]
ψ	stream function [$m^2 s^{-1}$]
η	similarity variable

Subscripts

w	condition at wall
∞	condition at free stream

Superscripts

$'$	derivative w.r.t. η

1. INTRODUCTION

In the modern world of brisk technology, one of the important requirements of industries is the cooling of the electronic devices. It is also observed in recent years that enhancement of heat transfer in mechanical and thermal systems are encountered. The classical heat transfer fluids like oil, ethylene, glycols and water have minimum thermal conductivity. For this purpose, an ingenious technique has been introduced to improve the heat transfer of thermal systems by suspending homogeneous mixture of ultrafine nanometer-sized (1-100 nm) particle in fluid which enhances the conventional heat transfer. These fluids are known as nanofluid. The latest progresses of their mathematical modeling and heat transfer nanofluids (Buongiorno, 2006) play a vital role in different industries. These types of fluids have various applications like hybrid power engines, heat exchanger, cooling of electronics, nuclear systems cooling, manufacturing, biomedicine, cooling and lubrication of machine parts etc. (Wong et al. 2009; Saidur et al. 2011). The aspect of enhancement the thermal conductivity by scattering nanoparticles in the fluid was scrutinized by Masuda et al. (1993). Khan and Pop (2005) obtained the numerical solution of nanofluid past a stretching sheet using Buongiorno's model and analyzed the Brownian motion and thermophoresis effects on heat transfer rate at the surface. Further, this problem was extended by Rana and Bhargava (2012) by considering nonlinear stretching sheet. Abbas et al. (2016) obtained the multiple solutions of non-linear radiative flow of a nanofluid past a contracting cylinder with thermophoretic diffusion and generalized slip condition. Recently, Anwar et al. (2016) explored the MHD flow of nanofluid near a stagnation point towards a nonlinear convectively heated stretching sheet with radiation effect and obtained the numerical solution using Keller-box method.

Recent studies of non-Newtonian fluid flow have presented a significant attention which is formed by moving plate. Because of bountiful modern and contemporary applications of non-Newtonian fluids like geographical streams, petroleum production, blood polymers, ink-jet printing, drilling muds, polymer handling, foods, etc. as a result lot of considerations has been paid them. There are collections of non-Newtonian fluids models are suggested by several researchers. Among several models, there is one of the important non-Newtonian model is Williamson fluid model. The Williamson fluid model has a definite advantage over other non-Newtonian fluid models in the sense that it contains both minimum viscosity $\tilde{\mu}_\infty$ and maximum viscosity $\tilde{\mu}_0$ which gives better results for pseudoplastic fluids (apparent viscosity at infinity does not tend to zero). In 1927, Williamson (1929) proposed this model which describe the equations of viscous flow of the pseudo-plastic fluids and verified the results experimentally. Nadeem et al. (2013) developed the two dimensional flow equations of Williamson fluid past a stretching surface and obtained the series solution using homotopy analysis method. Khan and Khan (2014) obtained the series solution of four types of steady flow of Williamson fluid. Nadeem and Hussain (2014) studied the heat transfer flow of a Williamson fluid past a stretching sheet moving exponentially. Kothandapani and Prakash (2015) explored the impacts of magnetic field and thermal radiation on the peristaltic transport of a non-Newtonian Williamson fluid in a tapered asymmetric channel containing nanoparticles. Malik and Salahuddin (2015) scrutinized the MHD flow of a Williamson fluid near a stagnation-point past a stretching cylinder and obtained the numerical solution. The influence of MHD on unsteady boundary layer flow of non-Newtonian Williamson fluid holding nanoparticles in a vertical channel immersed in porous medium in the presence of oscillating wall temperature was investigated by Immaculate et al. (2016). Recently, Krishnamurthy et al. (2016) scrutinized the influence of chemical reaction and MHD on flow with melting heat transfer of non-Newtonian Williamson fluid in porous medium containing nanoparticles.

Various systems dealing heat transfer with the mechanism of irreversibility which illustrates the entropy generation is correspond to mass transfer, viscous dissipation, heat transfer and magnetic field. Different researchers/scientist applied the second law of thermodynamics (Bejan, 1980; 1996). To optimize such kind of irreversibility for instance, Tasnim et al. (2002) examined the simultaneous the hydromagnetic effects and entropy generation through a vertical porous channel. Mahmud and Fraser (2004) considered the MHD free convection flow with entropy generation through a porous cavity. They determined that increment in a magnetic field leads to increase the entropy generation. Komurgoz et al. (2012) explored the entropy generation with the magnetic field towards the inclined porous planar channel. It was observed that maximum entropy generation can be obtained in absence of magnetic field and porosity. Butt and Ali (2013) studied the effects of entropy and thermal radiation in hydromagnetic free convection flow in vertical plated through a porous medium. Further investigation of entropy generation under the influence of MHD and slip flow on a rotating disk in a porous medium have variables properties was given by Rashidi et al. (2014). Recently, numerical study was conducted by Qing et al. (2016) on entropy generation. They discussed the Casson fluid flow over a stretching/shrinking porous sheet.

The process of mass transfer with binary chemical reaction and Arrhenius activation energy has been given a lot of attention due to its various applications in chemical engineering, cooling of nuclear reacting, geothermal reservoirs and recovery of thermal oil. Generally, the relations between chemical reactions and mass transport are very complex, and can be scrutinized in the utilization of reactant species and production at several rates within the mass transfer and fluid. Bestman (1990) was first who considered the combined effects of binary chemical reaction and Arrhenius activation energy on free convection flow with mass transfer in a vertical pipe immersed in a porous medium. He obtained the analytic solution using perturbation method. Srinivas and Muthuraj (2011) studied the combined effects of MHD and chemical reaction on mixed convective peristaltic flow with heat and mass transfer over a vertical permeable space. Maleque (2013a) studied MHD free convection flow and heat with mass transfer over a porous vertical plate with binary chemical reaction and Arrhenius activation energy with heat generation\absorption and viscous dissipation. Maleque (2013b) studied the MHD free convection flow over a permeable unsteady flat plate with exothermic/endothermic chemical reactions, Arrhenius activation energy and thermal radiation. The unsteady flow with heat and mass transfer past a stretching sheet with binary chemical reaction with Arrhenius activation energy in a rotating fluid was scrutinized by Awad et al. (2014). Muthuraj et al. (2016) investigated elasticity of flexible wall with heat and mass transfer on peristaltic transport of a dusty fluid with chemical reaction. Recently, Shafique et al. (2016) studied the steady flow of a non-Newtonian Maxwell fluid past an elastic surface in a rotating frame in the presence of binary chemical reaction along with activation energy.

In view of such facts, the prime interest of the current communication is to examine entropy generation on stagnation point flow of a Williamson nanofluid through a moving plate with activation energy and binary chemical reaction. In this study, Williamson fluid has been taken as a base fluid. The present flow problem is simplified with an appropriate use of transformation and solved by shooting method. The impacts of all physical parameters of interest are discussed numerically and graphically. To the author's best of knowledge, no one yet considered this type of problem.

2. PROBLEM FORMULATION

Consider a steady two-dimensional incompressible flow of a Williamson nanofluid past a moving plate with activation energy and binary chemical reaction. The *x*-axis is taking along the plate in the direction of motion and *y*-axis normal to it as shown in Fig. 1. The external free stream velocity of the plate is taken as $u_e(x) = cx$ where c is a positive constant. Moreover, T_w and C_w are the convective temperature and concentration of nanoparticle at the plate, while T_∞ and C_∞ are ambient temperature and ambient concentration of nanoparticle, respectively. The Cauchy stress tensor of Williamson fluid is given by (Nadeem et al. 2013; Nadeem and Hussain, 2014).

$$\Gamma = -pI + \Phi \,, \tag{1}$$

and

$$\Phi = \left(\tilde{\mu}_\infty + \frac{\tilde{\mu}_0 - \tilde{\mu}_\infty}{1 - \mathrm{X}\dot{\alpha}} \right) \tilde{A}_1 \,, \tag{2}$$

where Φ is the extra stress tensor, $\tilde{\mu}_0$ and $\tilde{\mu}_\infty$ are the limiting viscosities at zero and infinite shear stresses, respectively, $\mathrm{X}>0$ is a time constant, $\tilde{A}_1$ is the first Rivilin-Erickson tensor and $\dot{\alpha}$ is defined as

$$\dot{\alpha}=\sqrt{\frac{1}{2}\tilde{\pi}}\,,\ \tilde{\pi}=\mathrm{trace}\left(\tilde{A}_1^2\right). \tag{3}$$

Following Gorla and Gireesha (2016), we only consider the case for which

$\tilde{\mu}_\infty=0$, $\mathrm{X}\dot{\alpha}<1$.

Thus, we get

$$\Phi=\frac{\tilde{\mu}_0}{1-\mathrm{X}\dot{\alpha}}\tilde{A}_1 \tag{4}$$

or using binomial expansion

$$\Phi=\tilde{\mu}_0\left(1+\mathrm{X}\dot{\alpha}\right)\tilde{A}_1 \tag{5}$$

Under these assumptions, the basic equations that describe the physical situation along with the boundary layer approximations are given by

$$\frac{\partial u}{\partial x}+\frac{\partial v}{\partial y}=0\,, \tag{6}$$

$$u\frac{\partial u}{\partial x}+v\frac{\partial u}{\partial y}=u_e(x)\frac{du_e(x)}{dx}+\nu\frac{\partial^2 u}{\partial y^2}+\sqrt{2}\nu\mathrm{X}\frac{\partial u}{\partial y}\frac{\partial^2 u}{\partial y^2}\,, \tag{7}$$

$$u\frac{\partial T}{\partial x}+v\frac{\partial T}{\partial y}=\alpha\frac{\partial^2 T}{\partial y^2}+\Lambda\left[D_B\frac{\partial C}{\partial y}\frac{\partial T}{\partial y}+\left(\frac{D_T}{T_\infty}\right)\left(\frac{\partial T}{\partial y}\right)^2\right], \tag{8}$$

$$u\frac{\partial C}{\partial x}+v\frac{\partial C}{\partial y}=D_B\frac{\partial^2 C}{\partial y^2}+\left(\frac{D_T}{T_\infty}\right)\left(\frac{\partial^2 T}{\partial y^2}\right)-k_r^2\left(\frac{T}{T_\infty}\right)^n e^{-\frac{E_a}{\kappa T}}\left(C-C_\infty\right), \tag{9}$$

The corresponding boundary conditions are

$$u = 0,\ v = 0,\ T = T_w,\ C = C_w \text{ at } y = 0,$$
$$u \to u_e(x),\ T \to T_\infty,\ C \to C_\infty \text{ as } y \to \infty. \tag{10}$$

where u and v are the velocity components in the $x-$ and $y-$directions, respectively, ρ is the density, ν is the kinematic viscosity, $\alpha = k/(\rho c)_f$ is the thermal diffusivity, k is the fluid thermal conductivity, $(\rho c)_f$ is the heat capacitance of base fluid, T is the temperature, C is the concentration of nanoparticle, D_B and D_T are the coefficients of Brownian and thermophoresis diffusion, respectively, $\Lambda = (\rho c)_p/(\rho c)_f$ is the ratio between the effective heat capacity of the nanoparticle material and specific heat capacitance of the fluid, $k_r^2 (T/T_\infty)^n e^{-\frac{E_a}{\kappa T}}$ and κ are the modified Arrhenius function and the Boltzmann constant, respectively, where k_r^2 is the chemical reaction rate constant and n is the fitted rate constant lies between $-1 < n < 1$.

We introduce the following dimensionless variables:

$$\eta = y\sqrt{\frac{c}{\nu}},\ \psi = \sqrt{c\nu}\,x f(\eta),\ \theta(\eta) = \frac{T - T_\infty}{T_w - T_\infty},\ \phi(\eta) = \frac{C - C_\infty}{C_w - C_\infty}. \tag{11}$$

Here η is the similarity variable, ψ is the stream function.

In view of relation (11), Equations (7)-(10) are transformed into the following self-similar ordinary differential equations

$$f''' + ff'' - f'^2 + \gamma f'' f''' + 1 = 0, \tag{12}$$

$$\theta'' + \Pr f\theta' + \Pr Nb\theta'\phi' + \Pr Nt(\theta')^2 = 0, \tag{13}$$

$$\phi'' + Scf\phi' + \frac{Nt}{Nb}\theta'' - \beta Sc(1 + \delta\theta)^n \exp\left(-\frac{E}{1 + \delta\theta}\right)\phi = 0, \tag{14}$$

subject to the boundary conditions

$$f(0)=0,\ f'(0)=0,\ \theta(0)=1,\ \phi(0)=1,$$
$$f'(\infty)\to 1,\ \theta(\infty)\to 0,\ \phi(\infty)\to 0. \tag{15}$$

where prime denote differentiation with respect to η, $\gamma=\sqrt{2c}\mathrm{X}u_e/\sqrt{\nu}$ is the Williamson parameter, $Nb=\tau D_B\left(C_w-C_\infty\right)/\nu$ is the Brownian motion parameter, $Nt=\tau D_T\left(T_w-T_\infty\right)/T_\infty\nu$ is the thermophoresis parameter, $\Pr=\nu/\alpha$ is the Prandtl number, $E=E_a/\kappa T_\infty$ is the dimensionless activation energy, $\beta=k_r^2/c$ is the non-dimensional reaction rate, $\delta=\left(T_w-T_\infty\right)/T_\infty$ is the temperature difference parameter and $Sc=\nu/D_B$ is the Schmidt number.

The important physical quantities of interest are the skin friction coefficient, the Nusselt number and the Sherwood Number are written as

$$C_{fx}=\frac{\tau_w}{\rho u_e^2},\quad Nu_x=\frac{xq_w}{\alpha(T_w-T_w)},\ Sh_x=\frac{xm_w}{D_B(C_w-C_\infty)}, \tag{16}$$

where τ_w is the shear stress, q_w is the heat flux and m_w is the mass flux given as

$$\tau_w=\mu_0\left(\frac{\partial u}{\partial y}+\frac{\mathrm{X}}{\sqrt{2}}\left(\frac{\partial u}{\partial y}\right)^2\right)_{y=0},\ q_w=-\alpha\left(\frac{\partial T}{\partial y}\right)_{y=0},\ m_w=-D_B\left(\frac{\partial C}{\partial y}\right)_{y=0}, \tag{17}$$

Using (11), we get

$$C_f\,\mathrm{Re}_x^{1/2}=f''(0)+\frac{\gamma}{2}f''^2(0),\quad Nu_x\,\mathrm{Re}_x^{-1/2}=-\theta'(0),\ Sh_x\,\mathrm{Re}_x^{-1/2}=-\phi'(0). \tag{18}$$

where $\mathrm{Re}_x=xu_e/\nu$ is the Reynolds number.

3. ENTROPY GENERATION ANALYSIS

Entropy equation of viscous fluid is written as (Bhatti and Rashidi 2016; Bhatti et al., 2016)

$$S_{gen}'''=\frac{k}{T_\infty^2}\left(\frac{\partial T}{\partial y}\right)^2+\frac{\mu}{T_\infty}\left[\left(\frac{\partial u}{\partial y}\right)^2+\frac{\mathrm{X}}{\sqrt{2}}\left(\frac{\partial u}{\partial y}\right)^3\right]+\frac{RD}{C_\infty}\left(\frac{\partial C}{\partial y}\right)^2+\frac{RD}{T_\infty}\left(\frac{\partial T}{\partial y}\right)\left(\frac{\partial C}{\partial y}\right) \tag{19}$$

Volumetric entropy generation have three factors, (i) Heat Transfer Irreversibility (HTI) and (ii) Fluid friction Irreversibility (FFI) (iii) Diffusive Irreversibility. It is characterized as

$$S_0''' = \frac{k(\Delta T)^2}{L^2 T_\infty^2} \tag{20}$$

With the help of Equation (11), the entropy generation in dimensionless form can be written as:

$$N_G = \frac{S_{gen}'''}{S_0'''} = \frac{\mathrm{Re}\, B_r}{\Omega}\left(f''^2 + \frac{\gamma}{2} f''^3 \right) + \mathrm{Re}\,\theta'^2 + \mathrm{Re}\,\lambda\left(\frac{\varsigma}{\Omega}\right)^2 \phi'^2 + \mathrm{Re}\,\lambda\left(\frac{\varsigma}{\Omega}\right)\theta'\phi' \tag{21}$$

where $\Omega = \Delta T / T_\infty$ is the dimensionless temperature difference, $Br = \mu u_e^2 / k\Delta T$ the Brinkman number, $\mathrm{Re}_L = cL^2 / v$ is the Reynolds number based on the characteristic length, $\varsigma = \Delta C / C_\infty$ is the dimensionless concentration difference and $\lambda = RDC_\infty / k$ is the diffusive constant parameter.

4. SOLUTION PROCEDURE

In current study, a useful numerical technique namely shooting method has been employed to scrutinize the flow problem described by the transformed equations (12)-(15). The summary of shooting method widely used by many researchers (Bhattacharyya et al., 2011; Zaib et al., 2016) is given below:

First convert the equations (12)-(15) into IVP (initial value problem). Then select a suited finite value of $\eta \to \infty$, say η_∞. We have the set of following first order system

$$\left.\begin{aligned} f' &= p, \\ p' &= q, \\ q' &= \left(p^2 - fq - 1\right)/\left(1 + \gamma q\right), \end{aligned}\right\} \tag{22}$$

$$\left.\begin{aligned} \theta' &= z, \\ z' &= -\mathrm{Pr}\, fz - \mathrm{Pr}\, Nb\, zh - \mathrm{Pr}\, Nt\, z^2, \end{aligned}\right\} \tag{23}$$

$$\left.\begin{aligned} &\phi' = h, \\ &h' = -Scfh - \frac{Nt}{Nb}z' + \beta Sc\left(1+\delta\theta\right)^n \exp\left(\frac{-E}{1+\delta\theta}\right)\phi, \end{aligned}\right\} \qquad (24)$$

under the boundary conditions

$$f(0) = 0,\ p(0) = 0,\ \theta(0) = 1,\ \phi(0) = 1. \qquad (25)$$

To solve the system of equations as an IVP we require the values for $q(0)$ i.e. $f''(0)$, $z(0)$ i.e. $\theta'(0)$ and $h(0)$ i.e. $\phi'(0)$ but there is no such values are given. The values of initial value for $f''(0)$, $\theta'(0)$ and $\phi'(0)$ are selected and the Runge–Kutta fourth order method is implemented to get a solution. Then the calculated values of $f'(\eta)$, $\theta(\eta)$ and $\phi(\eta)$ at η_∞(=8) are compared under the known boundary conditions $f'(\eta_\infty) = 1$, $\theta(\eta_\infty) = 0$ and $\phi(\eta_\infty) = 0$. The step size is taken as $\Delta\eta = 0.01$. The technique is repeated until we obtain results correct up to the desired accuracy of the 10^{-5} level, which fulfills the convergence criterion.

5. ANALYSIS

Tables 1 and 2 are arranged for comparison of the present results with the previous published results in the limiting case. It is observed that the present results are matched closely, which assured the validity of the current methodology. Table 3 presents the values of the Nusselt number as well as the Sherwood number for different values of γ versus Nb. The Nusselt number is rapidly decreases with increasing Nb while promptly increasing behavior is seen for Sherwood number. Figs. 2-4 are prepared to show the impact of Williamson parameter γ on the velocity profile, temperature distribution and concentration of nanoparticle. The velocity profile shows a decreasing behavior with increasing values of γ and develops the thicker velocity boundary layer as sketched in Fig. 2. Moreover, the thickness of velocity boundary layer is smaller for Newtonian nanofluid $(\gamma = 0)$ compared to non-Newtonian nanofluid $(\gamma \neq 0)$. Figs. 3

and 4 envisage that the temperature distribution and concentration of nanoparticle as well as thermal and concentration boundary layers thicknesses increase as increase in the value of γ.

The impact of thermophoresis parameter Nt on the temperature distribution and concentration profile are presented in Figs. 5 and 6, respectively. Figs. 5 and 6 reveal that the temperature distribution and concentration of nanoparticle enhance due to increasing values of Nt. This is because diffusion penetrates deeper into the fluid due to increasing values of Nt which causes the thickening of the thermal boundary layer as well as the concentration boundary layer. Since increase in Nt corresponds to the increase in thermophoretic diffusion coefficient which ultimately enhancing the concentration of nanoparticle. It is interesting to note that the effect of thermophoresis parameter is more pronounced on the concentration of nanoparticle compared to temperature distribution.

Figs. 7 and 8 are prepared to see the Brownian motion effect Nb on the temperature distribution and concentration of nanoparticle, respectively. Fig. 7 elucidates that the temperature distribution and thermal boundary layer thickness increase with increasing Nb. Physical reason is that the kinetic energy of the nanoparticles increases due to the strength of this chaotic motion and as a result, the fluid's temperature increases. Whereas, the opposite trend is seen on the concentration profile as depicted in Fig. 8. It can be seen that the concentration of nanoparticle gradually decreases due to increasing values of Nb. It can be concluded that the Brownian motion parameter makes the fluid warm within the boundary and at that time aggravates deposition particles away from the regime of fluid to the surface that causing in a decrease in concentration profile as well as the thickness of boundary layer. The larger values of Brownian motion imply the strong behavior for the smaller particle, whereas for stronger particle the smaller values of Nb applied.

Fig. 9 preserves the influence of temperature difference δ on the concentration of nanoparticle. This result showed that the concentration of nanoparticle and concentration boundary layer thickness compress due to increasing values of δ. Fig. 10 envisages that due to increasing values of dimensionless reaction rate β, the concentration of nanoparticle shrinkage and leads to thinning the concentration boundary layer thickness. Physically, an increase in the value of β leads an increase in the term $\beta(1+\delta\theta)^n \exp(-E/1+\delta\theta)$. This ultimately helps the destructive chemical reaction that increases the concentration. The contraction in ϕ is followed with a higher gradient of concentration at the plate. Fig. 11 elucidates that the concentration of nanoparticle and concentration boundary layer thickness are increasing function of non-dimensional activation energy E. This ultimately advances the generative chemical reaction due to which nanoparticle concentration enhances. Physically, higher activation energy and lower temperature leads to lesser reaction rate which slowdown the chemical reaction and thus concentration of nanoparticle enhances. Moreover, it is noticed from these figures that the profile of concentration of nanoparticles is higher in presence of activation energy $(E \neq 0)$ compared to absence of activation energy $(E = 0)$, while the opposite trend is observed in cases of temperature difference and reaction rate.

Figs. 12-14 elaborate the variation of entropy generation against Williamson parameter γ, Reynolds number Re_L and Brinkman number Br. Fig. 12 envisages that the entropy profile initially shows a decreasing behavior with increasing γ and then starting to increase after a certain value of η. As expected, the entropy generation profile is higher for non-Newtonian fluid compared to Newtonian fluid. We observed from Figs. 13 and 14 that entropy profile accelerates by increasing either Brinkman number or Reynolds number. Since the entropy generation generated from mechanisms of all irreversibilities and as a result the entropy generation increases with increasing Re_L. Larger values in entropy generation created by the irreversibility of fluid friction occur due to increasing Br.

Figs. 15 and 16 are set to scrutinize the effect of γ versus Nb on the Nusselt number and the Sherwood number. These figures show the decreasing behavior with increasing values of γ. It is also observed from Fig. 15 that the values of Nusselt number decreases rapidly as the values of Nb increases. Whereas, the values of Sherwood number increases quiet significantly with increasing Nb as illustrated in Fig. 16. Moreover, it is worth mentioning that the values of the Nusselt number and the Sherwood number are positive. Physically, positive values of the Nusselt number means that heat is moved from hot place to the cold fluid. Finally, the sketched of streamlines using stream function ψ are illustrated in Figs. 17. This figure signifies that streamlines are moderately simple, symmetric and fuller towards an axis.

6. CONCLUDING REMARKS

In the present perusal, optimization of entropy generation with activation energy and binary chemical reaction on stagnation point flow of a non-Newtonian Williamson fluid over a moving plate has been investigated. Suitable transformations have been applied to model the governing flow problem. The numerical results of the governing flow problem are obtained by using shooting method. The expression of entropy generation was obtained as a function of temperature distribution, velocity and concentration gradient. The important outcomes for the current analysis are:

- The velocity of fluid decreases due to higher values of γ and temperature distribution and concentration of nanoparticle increase with γ.

- Temperature distribution and concentration of nanoparticle increase as the thermophoresis parameter increases.
- Due to increasing values of Brownian motion parameter leads to increase the temperature of fluid and decreases the concentration of nanoparticle.
- Entropy profile is increased due to the greater impact of Williamson parameter, Reynolds number and Brinkman number.
- The values of Nusselt number and Sherwood number are decrease when γ increases.
- Streamlines are fuller and moderately simple, symmetric towards an axis.

ACKNOWLEDGMENT

We wish to express sincere thanks to the reviewers for their valuable comments and suggestions.

REFERENCES

Abbas, Z., Perveen, P., Sheikh, M., and Pop, I., Thermophoretic Diffusion and Nonlinear Radiative Heat Transfer due to a Contracting Cylinder in a Nanofluid with Generalized Slip Condition, *Results Phys*., vol. **6,** pp. 1080–1087, 2016.

Anwar, M.I., Shafie, S., Kasim, A.R.M., and Salleh, M.Z., Radiation Effect on MHD Stagnation-Point Flow of a Nanofluid over a Nonlinear Stretching Sheet with Convective Boundary Condition, *Heat Trans. Res*., vol. **47**, no. 9, pp. 797–816, 2016.

Awad, F.G., Motsa, S., and Khumalo, M., Heat and Mass Transfer in Unsteady Rotating Fluid Flow with Binary Chemical Reaction and Activation Energy, *PLoS ONE*, vol. **9,** pp. 1–12, 2014.

Bejan, A., Second Law Analysis in Heat Transfer. *Energy*, vol. **5**, pp. 720–732, 1980.

Bejan, A., *Entropy generation minimization: The method of thermodynamic optimization of finite-size systems and finite-time processes*, CRC Press, 1996.

Bestman, Natural Convection Boundary Layer with Suction and Mass Transfer in a Porous Medium, *Int. J. Eng. Res*., vol. **14**, pp. 389–396, 1990.

Bhatti, M.M. and Rashidi, M.M., Numerical Simulation of Entropy Generation on MHD Nanofluid towards a Stagnation Point Flow over a Stretching Surface, *Int. J. Appl. Comput. Math.*, vol. **3,** no. 3, pp. 2275**–**2289, 2016.

Bhatti, M.M., Abbas, T., Rashidi, M.M., Ali, M.E.S., and Yang, Z., Entropy Generation on MHD Eyring–Powell Nanofluid Through a Permeable Stretching Surface, *Entropy*, vol. **18,** pp. 1**–**14, 2016.

Bhattacharyya, K. and Layek, G.C., Effects of Suction/Blowing on Steady Boundary Layer Stagnation-Point Flow and Heat Transfer towards a Shrinking Sheet with Thermal Radiation, *Int. J. Heat Mass Trans*., vol. **54,** pp. 302–307, 2011.

Buongiorno, J., Convective Transport in Nanofluids, *ASME J. Heat Trans*., vol. **128,** pp. 240–250, 2006.

Butt, A.S. and Ali, A., Entropy Effects in Hydromagnetic Free Convection Flow past a Vertical Plate Embedded in a Porous Medium in the Presence of Thermal Radiation, *Europ. Phy. J. Plus*, vol. **128,** pp. 51–55, 2013.

Galanis, N. and Rashidi, M.M., Entropy Generation in Non-Newtonian Fluids due to Heat and Mass Transfer in the Entrance Region of Duct, *Heat Mass Trans*., vol. **48,** pp. 1647**–**1662, 2012.

Gorla, R.S.R. and Gireesha, B.J., Dual Solutions for Stagnation‑Point Flow and Convective Heat Transfer of a Williamson Nanofluid past a Stretching/Shrinking Sheet, *Heat Mass Trans*., vol. **52,** pp. 1153–1162, 2016.

Hamad, M.A.A., Uddin, Md. J., and Ismail, M.I.Md., Radiation Effects on Heat and Mass Transfer in MHD Stagnation-Point Flow over a Permeable Flat Plate with Thermal Convective Surface

Boundary Condition, Temperature Dependent Viscosity and Thermal Conductivity, *Nuclear Eng. Design*, vol. **242,** pp. 194–200, 2012.

Immaculate, D.L., Muthuraj, R., Shukla, A.K., and Srinivas, S., MHD Unsteady Flow of a Williamson Nanofluid in a Vertical Porous Space with Oscillating Wall Temperature, *Front. Heat Mass Trans.*, vol. **7,** no. 12, pp. 1–14, 2016.

Khan, W.A. and Pop, I., Boundary-layer Flow of a Nanofluid past a Stretching Sheet, *Int. J. Heat Mass Trans*., vol. **53,** pp. 2477–2483, 2010.

Khan, W.A. and Pop, I., Boundary Layer Flow past a Wedge Moving in a Nanofluid, *Math. Prob. Eng*., vol. **2013,** pp. 1–7, 2013.

Khan, N.A. and Khan, H., A boundary Layer Flows of Non-Newtonian Williamson Fluid, *Nonlinear Eng*., vol. **3,** pp. 107–115, 2014.

Komurgoz, G., Arikoglu, A., and Ozkol, I., Analysis of the Magnetic Effect on Entropy Generation in an Inclined Channel Partially filled with Porous Medium, *Num. Heat Trans. Part A: Appl*., vol. **61,** pp. 786–799, 2012.

Kothandapani, M. and Prakash, J., Effects of Thermal Radiation Parameter and Magnetic Field on the Peristaltic Motion of Williamson Nanofluids in a Tapered Asymmetric Channel, *Int. J. Heat Mass Trans.*, vol. **81,** pp. 234–245, 2015.

Krishnamurthy, M.R., Prasannakumara, B.C., Gireesha, B.J., and Gorla, R.S.R., Effect of Chemical Reaction on MHD Boundary Layer Flow and Melting Heat Transfer of Williamson Nanofluid in Porous Medium, *Eng. Sci. Tech. Int. J*., vol. **19,** pp. 53–61, 2016.

Kuo, B.L., Heat Transfer Analysis for the Falkner-Skan Wedge Flow by the Differential Transformation Method, *Int. J. Heat Mass Trans*., vol. **48,** pp. 5036–5046, 2005.

Mahian, O., Mahmud, S., and Heris, S.Z., Analysis of Entropy Generation between Co-Rotating

Cylinders using Nanofluids, *Energy*, vol. **44,** pp. 438–446, 2012.

Mahmud, S. and Fraser, R.A., Magnetohydrodynamic Free Convection and Entropy Generation in a Square Porous Cavity, *Int. J. Heat Mass Trans*., vol. **47,** pp. 3245–3256, 2004.

Maleque, Kh.A., Effects of Binary Chemical Reaction and Activation Energy on MHD Boundary Layer Heat and Mass Transfer Flow with Viscous Dissipation and Heat Generation/ Absorption, *ISRN Thermodyn*., vol. **2013,** pp. 1–7, 2013a.

Maleque, Kh.A., Effects of Exothermic/Endothermic Chemical Reactions with Arrhenius Activation Energy on MHD Free Convection and Mass Transfer Flow in Presence of Thermal Radiation, *J. Thermodyn*., vol. **2013,** pp. 1–11, 2013b.

Malik, M.Y. and Salahuddin, T., Numerical Solution of MHD Stagnation Point Flow of Williamson Fluid Model over a Stretching Cylinder, *Int. J. Nonlinear Sci. Num. Simul*., vol. **16,** pp. 161–164, 2015.

Masuda, H., Teramae, A.E.K., and Hishinuma, N., Alteration of Thermal Conductivity and Viscosity of Liquid by Dispersing Ultra-Fine Particles, *Netsu Bussei*, vol. **7,** pp. 227–233, 1993.

Muthuraj, R., Nirmala, K., and Srinivas, S., Influences of Chemical Reaction and Wall Properties on MHD Peristaltic Transport of a Dusty Fluid with Heat and Mass Transfer, *Alexandria Eng. J*., vol. **55,** pp. 597–611, 2016.

Nadeem, S. and Hussain, S.T., Heat Transfer Analysis of Williamson Fluid over Exponentially Stretching Surface, *Appl. Math. Mech. -Engl. Ed*., vol. **35,** pp. 489–502, 2014.

Nadeem, S., Hussain, S.T., and Lee, C., Flow of a Williamson Fluid over a Stretching Sheet, *Braz. J. Chem. Eng*., vol. **30,** pp. 619–625, 2013.

Qing, J., Bhatti, M.M., Abbas, M.A., Rashidi, M.M., and Ali, M.E.S., Entropy Generation on MHD Casson Nanofluid Flow over a Porous Stretching/Shrinking surface, *Entropy*, vol. **18,** pp. 1–

14, 2016.

Rana, P. and Bhargava, R., Flow and Heat Transfer of a Nanofluid over a Non-Linearly Stretching Sheet: a Numerical Study, *Commun. Nonlin. Sci. Num. Simul*., vol. **17,** pp. 212–226, 2012.

Rashidi, M.M., Kavyani, N., and Abelman, S., Investigation of Entropy Generation in MHD and Slip Flow over a Rotating Porous Disk with Variable Properties, *Int. J. Heat Mass Trans*., vol. **70,** pp. 892–917, 2014.

Saidur, R., Leong, K.Y., and Mohammad, H.A., A Review on Applications and Challenges of Nanofluids, *Renew. Sustain. Energy Rev*., vol. **15,** pp. 1646–1648, 2011.

Shafique, Z., Mustafa, M., and Mushtaq, A., Boundary Layer Flow of Maxwell Fluid in Rotating Frame with Binary Chemical Reaction and Activation Energy, *Results Phys*., vol. **6,** pp. 627–633, 2016.

Srinivas, S. and Muthuraj, R., Effects of Chemical Reaction and Space Porosity on MHD Mixed Convective Flow in a Vertical Asymmetric Channel with Peristalsis, *Math. Comp. Model*., vol. **54,** pp. 1213–1227, 2011.

Tasnim, S.H., Shohel, M., and Mamun, M.A.H., Entropy Generation in a Porous Channel with Hydromagnetic Effect, *Int. J. Exergy*, vol. **2,** pp. 300–308, 2002.

Williamson, R.V., The Flow of Pseudoplastic Materials, *Industrial Eng. Chem. Res*., vol. **21,** pp. 1108–1111, 1929.

Wong, K.V. and Leon, O.D., Application of Nanofluids: Current and Future, *J. Adv. Mech. Eng*., vol. **2,** pp. 1–11, 2009.

Yacob, N.A., Ishak, A., and Pop, I., Falkner-Skan Problem for a Static or Moving Wedge in Nanofluids, *Int. J. Therm. Sci*., vol. **50,** pp. 133–139, 2011.

Zaib, A., Bhattacharyya, K., Sharif, U.Md., and Shafie, S., Dual Solutions of Non-Newtonian Casson Fluid Flow and Heat Transfer over an Exponentially Permeable Shrinking Sheet with Viscous Dissipation, *Modelling Simulat. Eng*., vol. **2016,** pp. 1–8, 2016.

TABLE 1: Comparison of the value of $f''(0)$ when $\gamma = 0$

Yacob et al. (2011)	**Hamad et al. (2012)**	**Present**
1.2326	1.232588	1.2326

TABLE 2: Comparison of the value of $-\theta'(0)$ when $\gamma = Nb = Nt = 0,\ \Pr = 6.2$

Kuo (2005)	**Khan and Pop (2013)**	**Present**
1.1147	1.1279	1.1280

TABLE 3: Values of the Nusselt number and the Sherwood number versus Nb for different values of γ when $Nt = 0.1,\ \Pr = 1,\ Sc = 1,\ E = 4,\ \beta = 3,\ \delta = 0.5,\ n = 0.5$ are fixed

γ	Nb	$Nu_x \mathrm{Re}_x^{-1/2}$	$Sh_x \mathrm{Re}_x^{-1/2}$
0	0.2	0.4936	0.6233
0	0.4	0.4418	0.6706
	0.6	0.3941	0.6870
1	0.2	0.4713	0.6089
	0.4	0.4217	0.6527
	0.6	0.3760	0.6679
2	0.2	0.4581	0.6004
	0.4	0.4098	0.6422
	0.6	0.3653	0.6568
3	0.2	0.4486	0.5943
	0.4	0.4011	0.6346
	0.6	0.3575	0.6488

FIG. 1: Physical diagram of the problem

FIG. 2: Velocity profile for different values of γ

FIG. 3: Temperature profile for different values of γ when $Nb = Nt = 0.5,\ \Pr = 1$

FIG. 4: Concentration of nanoparticle for different values of γ when $Nb = Nt = 0.5,$

$Sc = 1,\ \beta = 8,\ E = 10,\ n = 0.5,\ \delta = 0.5$

FIG. 5: Temperature profile for different values of Nt when $\gamma = 0.2,\ Nb = 1.5,\ \Pr = 1$.

FIG. 6: Concentration of nanoparticle for different values of Nt when $\gamma = 0.2,\ Nb = 0.5,$

$Sc = 1,\ \beta = 3,\ E = 4,\ n = 0.5,\ \delta = 0.5$

FIG. 7: Temperature profile for different values of Nb when $\gamma = 0.2,\ Nt = 0.1,\ \Pr = 1$

FIG. 8: Concentration of nanoparticle for different values of Nb when $\gamma = 0.2,\ Nt = 0.1,$

$Sc = 1,\ \beta = 3,\ E = 4,\ n = 0.5,\ \delta = 0.5$

FIG. 9: Concentration of nanoparticle for different values of δ when $\gamma = 0.2,\ Nt = 0.1,\ Nb = 0.5,$

$Sc = 1,\ \beta = 3,\ E = 4,\ n = 0.5$

FIG. 10: Concentration of nanoparticle for different values of β when

$\gamma = 0.2,\ Nt = 0.1,\ Nb = 0.5,\ Sc = 1,\ \delta = 0.5,\ E = 4,\ n = 0.5$

FIG. 11: Concentration of nanoparticle for different values of E when

$\gamma = 0.2,\ Nt = 0.1,\ Nb = 0.5,\ Sc = 1,\ \delta = 0.5,\ \beta = 3,\ n = 0.5$

FIG. 12: Entropy generation for different values of γ when $Nb = Nt = 0.5,$

$Sc = 1,\ \beta = 3,\ E = 4,\ n = 0.5,\ \delta = 0.5,\ \mathrm{Re} = Br = 1,\ \varsigma = 0.1,\ \lambda = \Omega = 0.01$

FIG. 13: Entropy generation for different values of Re_L when $Nt = 0.1, Nb = 0.5,$

$\gamma = 0.2,\ Sc = 1,\ \beta = 3,\ E = 4,\ n = 0.5,\ \delta = 0.5,\ Br = 1,\ \varsigma = 0.1,\ \lambda = \Omega = 0.01$

FIG. 14: Entropy generation for different values of Br when $Nt = 0.1, Nb = 0.5,$

$\gamma = 0.2,\ Sc = 1,\ \beta = 3,\ E = 4,\ n = 0.5,\ \delta = 0.5,\ \mathrm{Re}_L = 1,\ \varsigma = 0.1,\ \lambda = \Omega = 0.01$

FIG. 15: Nusselt number versus Nb for different values of γ when $Nt = 0.1,\ \mathrm{Pr} = 1$

FIG. 16: Sherwood number versus Nb for different values of γ when $\gamma = 0.2,\ Nt = 0.1,$

$\beta = 3,\ Sc = 1,\ \delta = 0.5,\ E = 4,\ n = 0.5$

FIG. 17: Streamline pattern when $\gamma = 1$

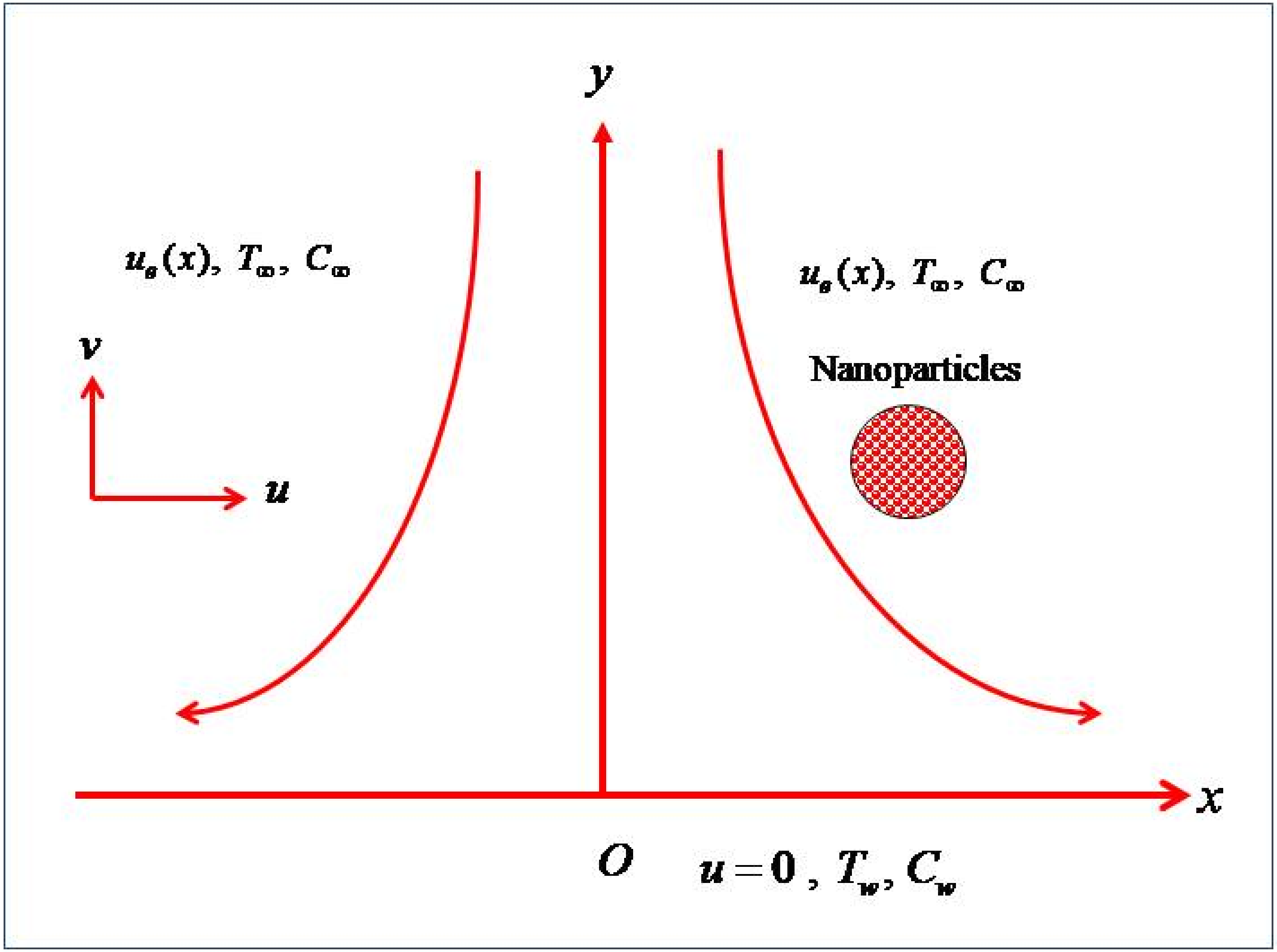

y
$u_e(x)$, T_∞, C_∞
$u_e(x)$, T_∞, C_∞
v
u
Nanoparticles
x
O
$u=0$, T_w, C_w

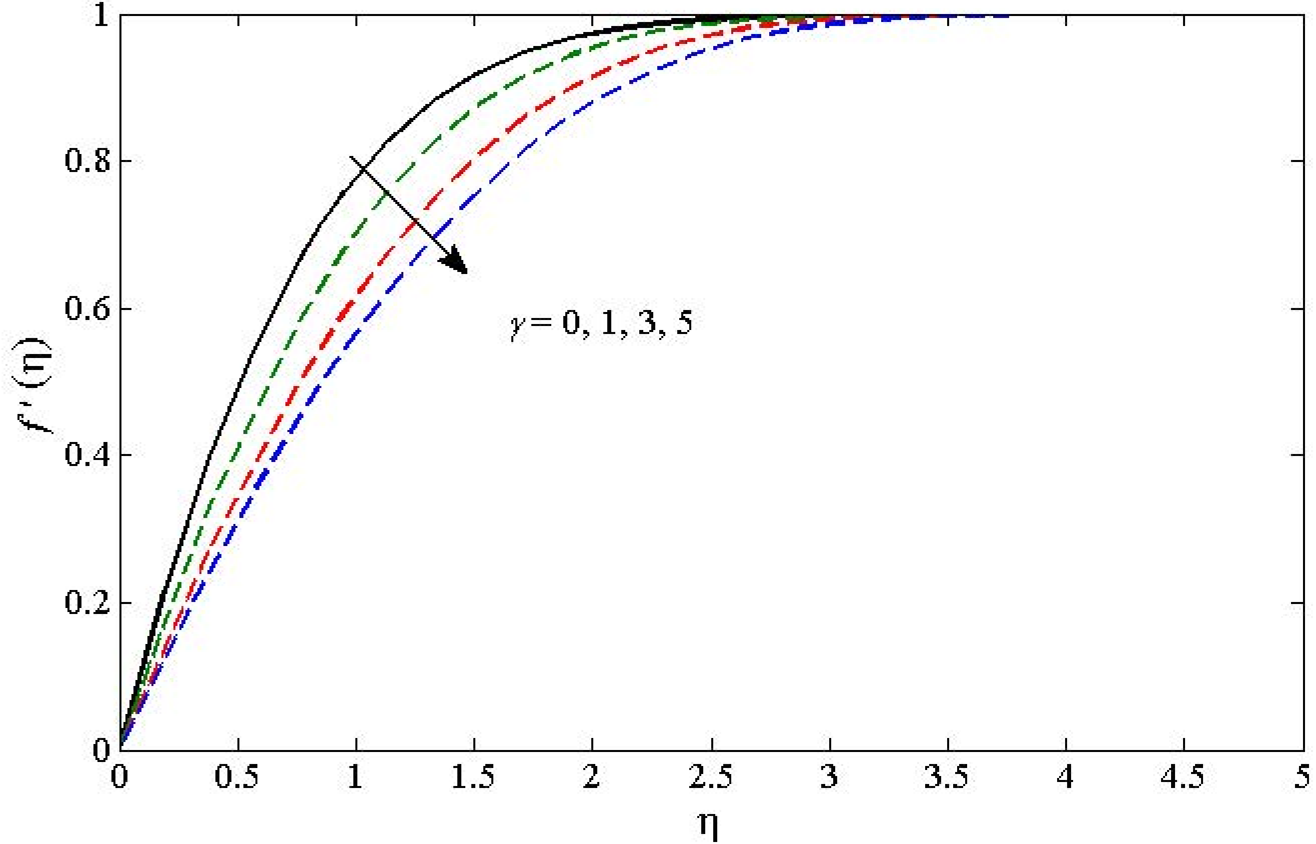

1
0.8
0.6
0.4
0.2
0
f ′ (η)
γ = 0, 1, 3, 5
0
0.5
1
1.5
2
2.5
3
3.5
4
4.5
5
η

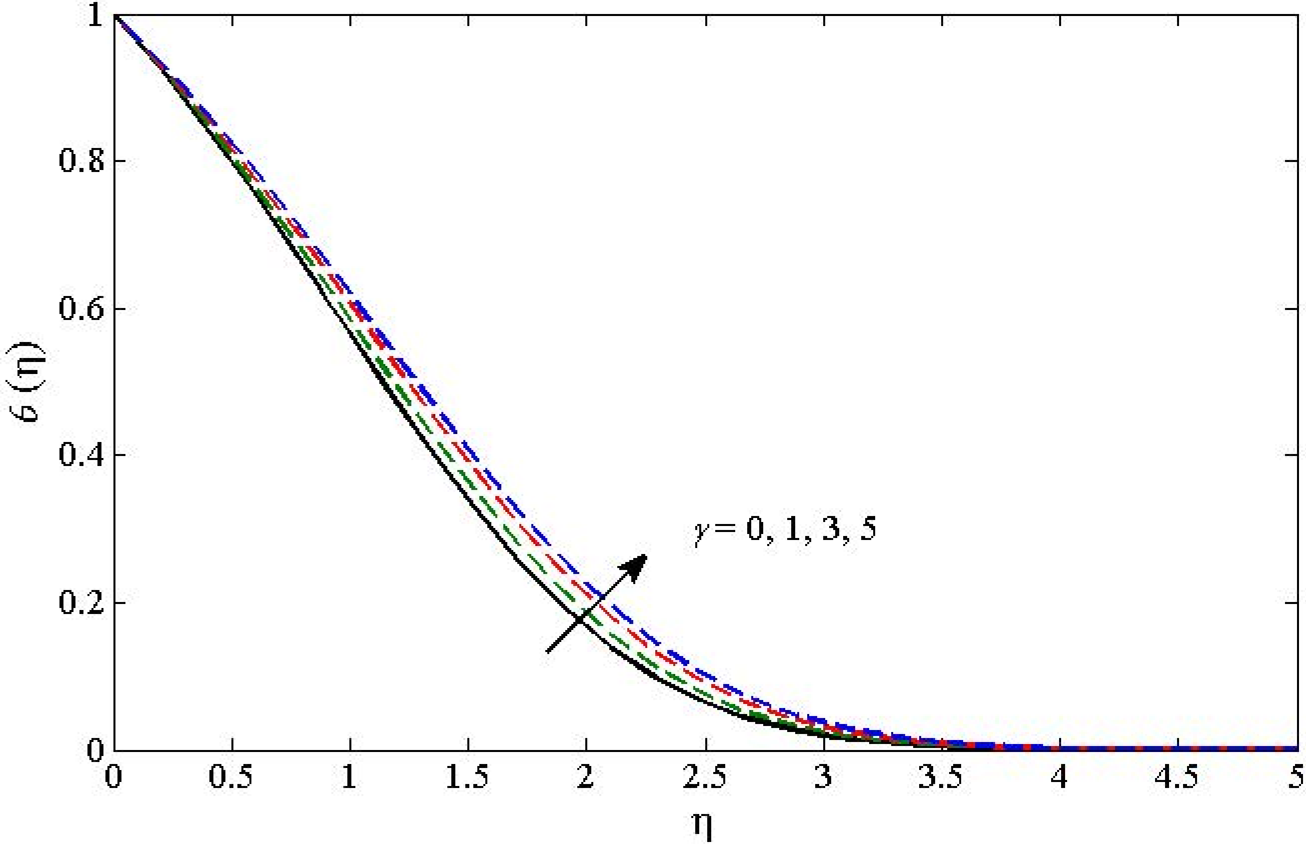

1
0.8
0.6
0.4
0.2
0
0
0.5
1
1.5
2
2.5
3
3.5
4
4.5
5
θ (η)
η
γ = 0, 1, 3, 5

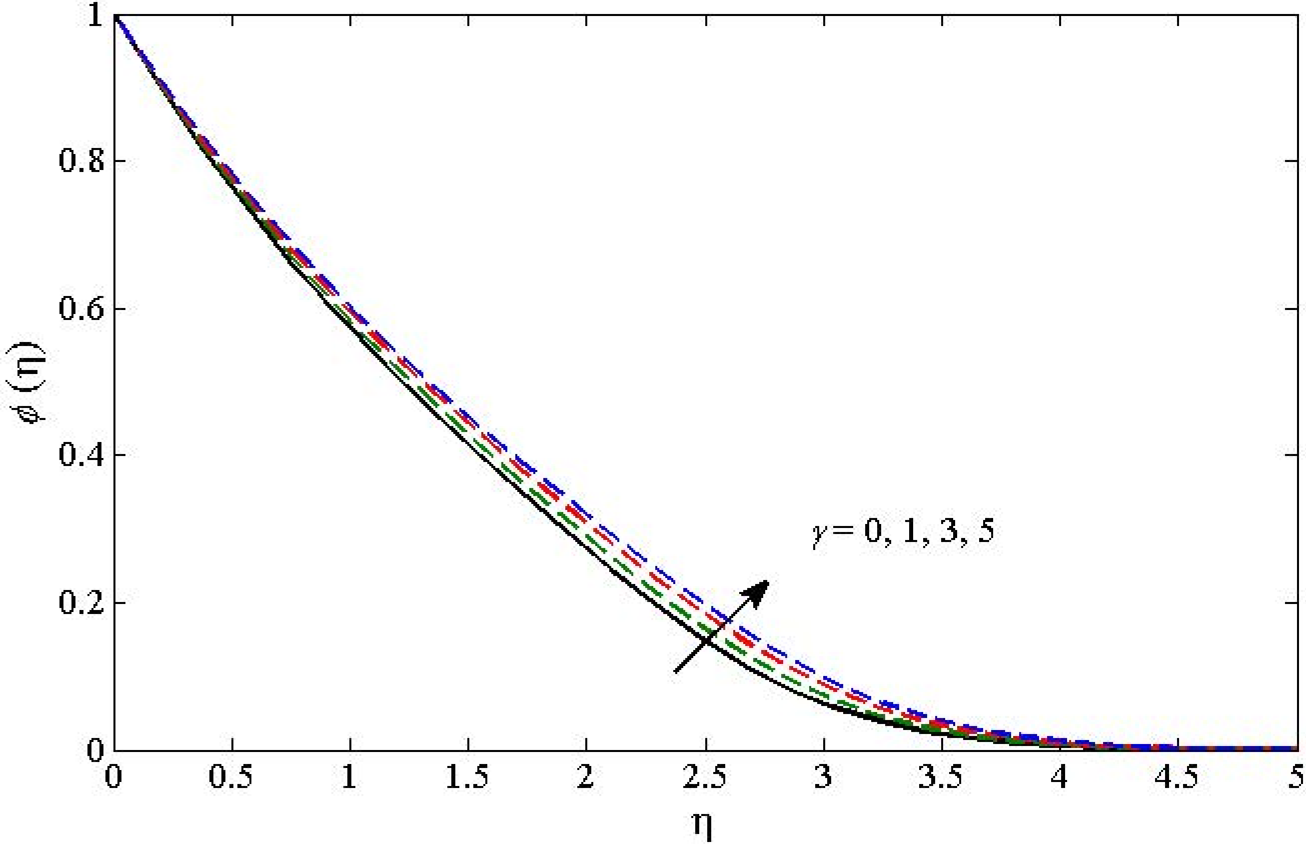

1
0.8
0.6
0.4
0.2
0
φ (η)
0
0.5
1
1.5
2
2.5
3
3.5
4
4.5
5
η
γ = 0, 1, 3, 5

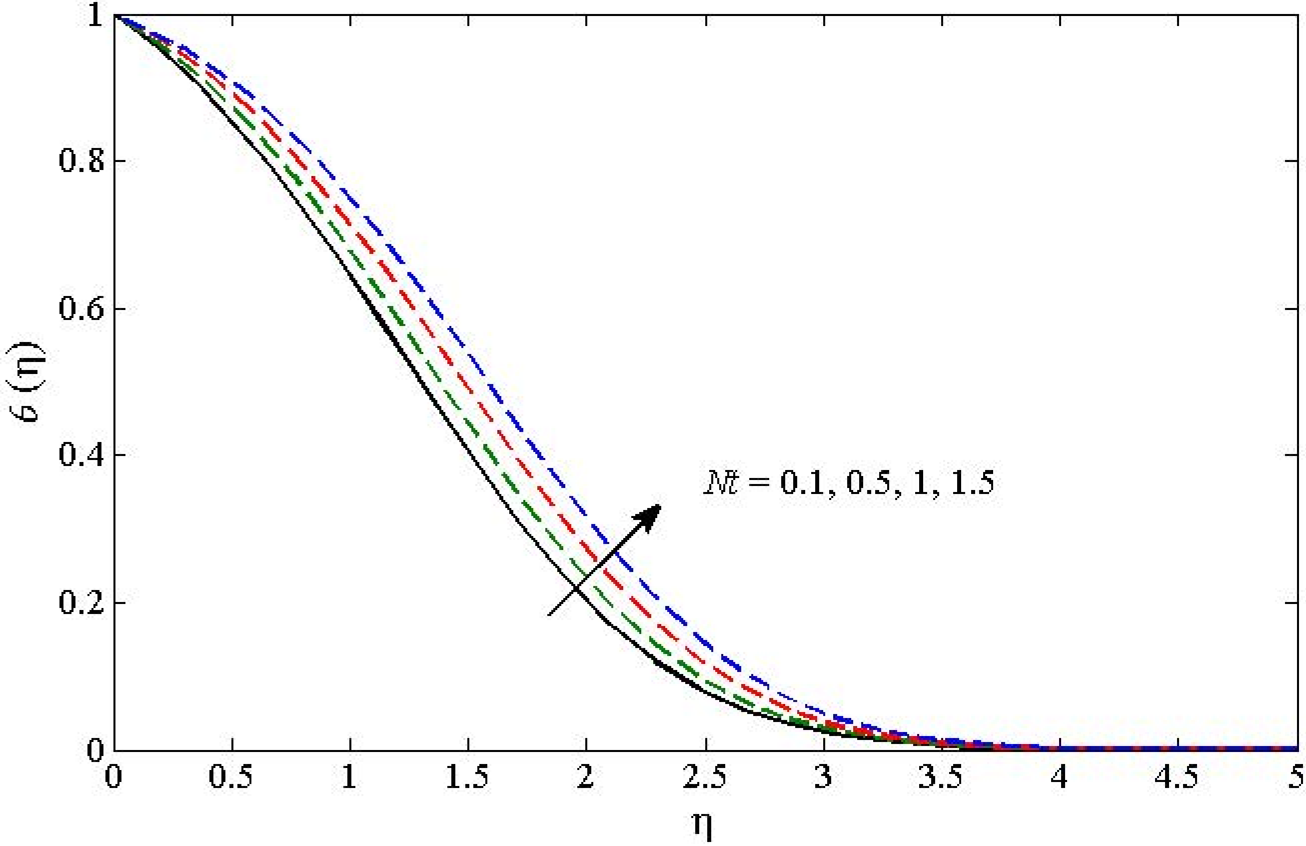

1
0.8
0.6
0.4
0.2
0
θ (η)
0
0.5
1
1.5
2
2.5
3
3.5
4
4.5
5
η
Nt = 0.1, 0.5, 1, 1.5

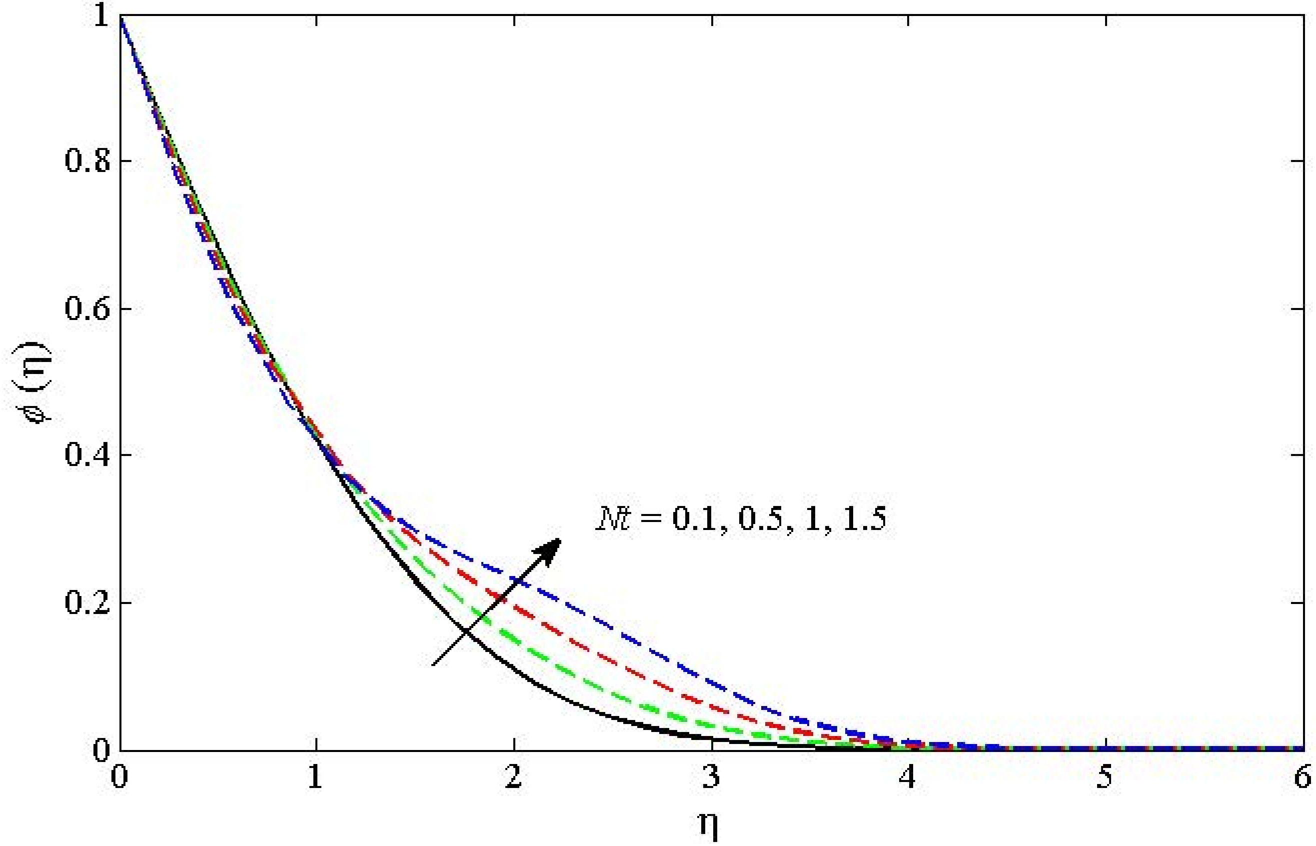

1
0.8
0.6
0.4
0.2
0
ϕ (η)
0
1
2
3
4
5
6
η
Nt = 0.1, 0.5, 1, 1.5

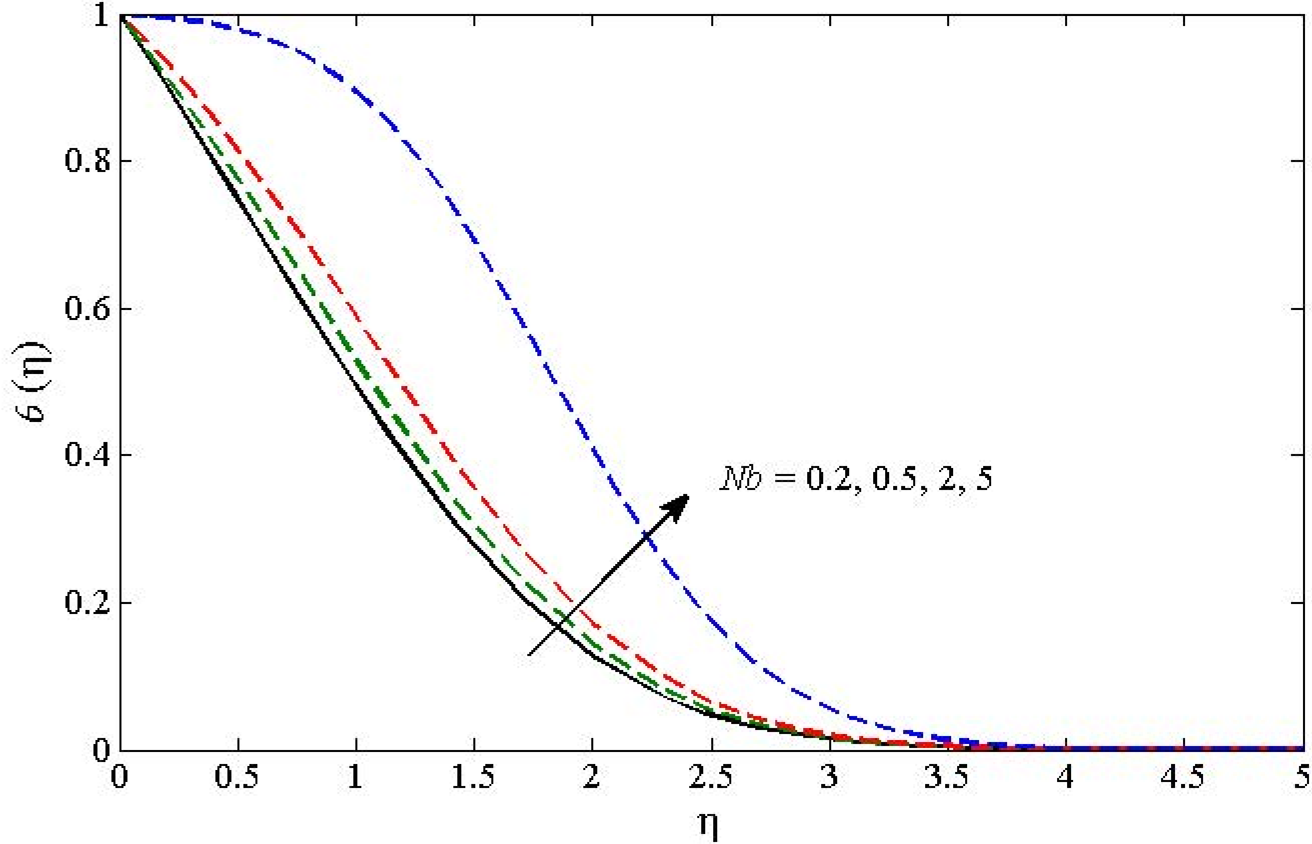

1
0.8
0.6
0.4
0.2
0
θ (η)
0
0.5
1
1.5
2
2.5
3
3.5
4
4.5
5
η
Nb = 0.2, 0.5, 2, 5

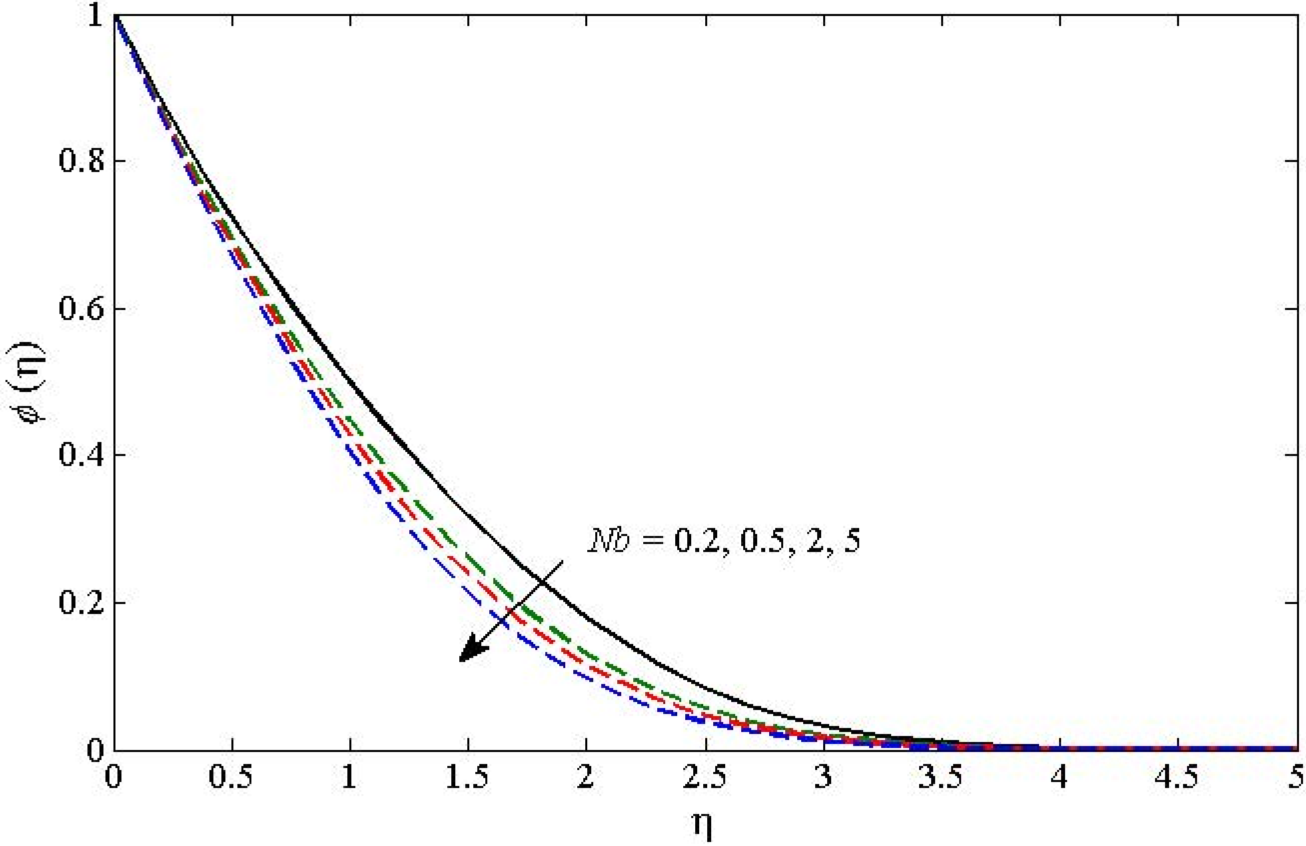

1
0.8
0.6
0.4
0.2
0
ϕ (η)
0
0.5
1
1.5
2
2.5
3
3.5
4
4.5
5
η
Nb = 0.2, 0.5, 2, 5

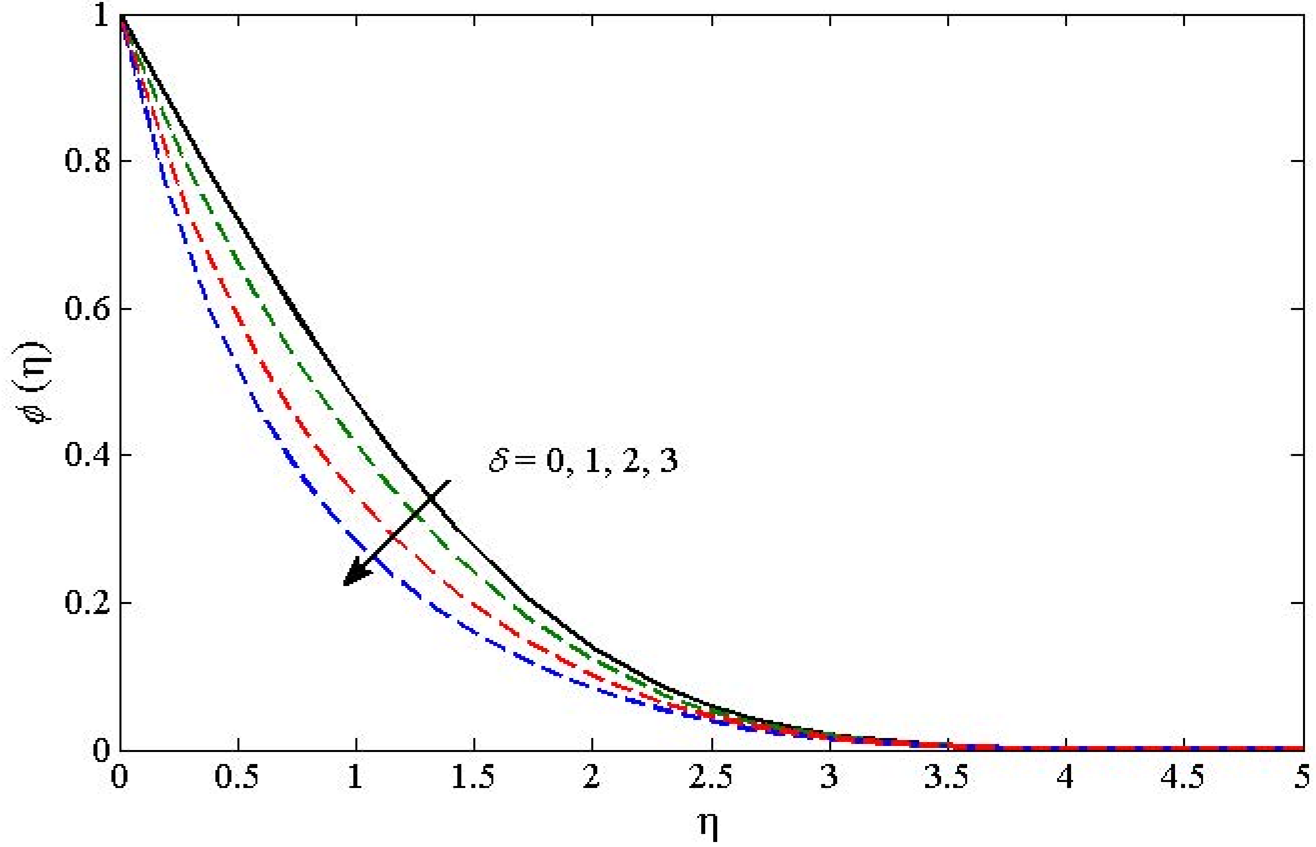

1
0.8
0.6
0.4
0.2
0
ϕ (η)
δ = 0, 1, 2, 3
0
0.5
1
1.5
2
2.5
3
3.5
4
4.5
5
η

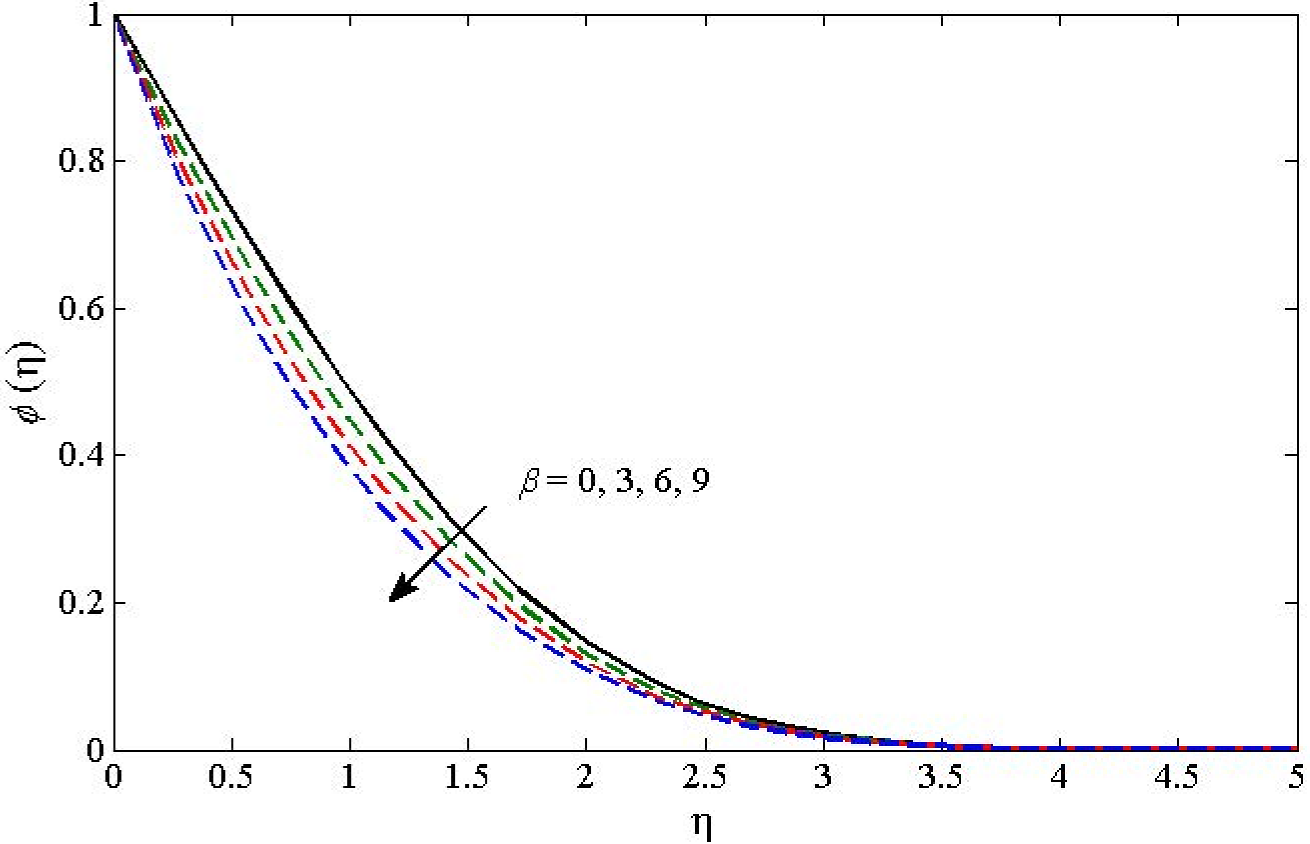

1
0.8
0.6
0.4
0.2
0
ϕ (η)
β = 0, 3, 6, 9
0
0.5
1
1.5
2
2.5
3
3.5
4
4.5
5
η

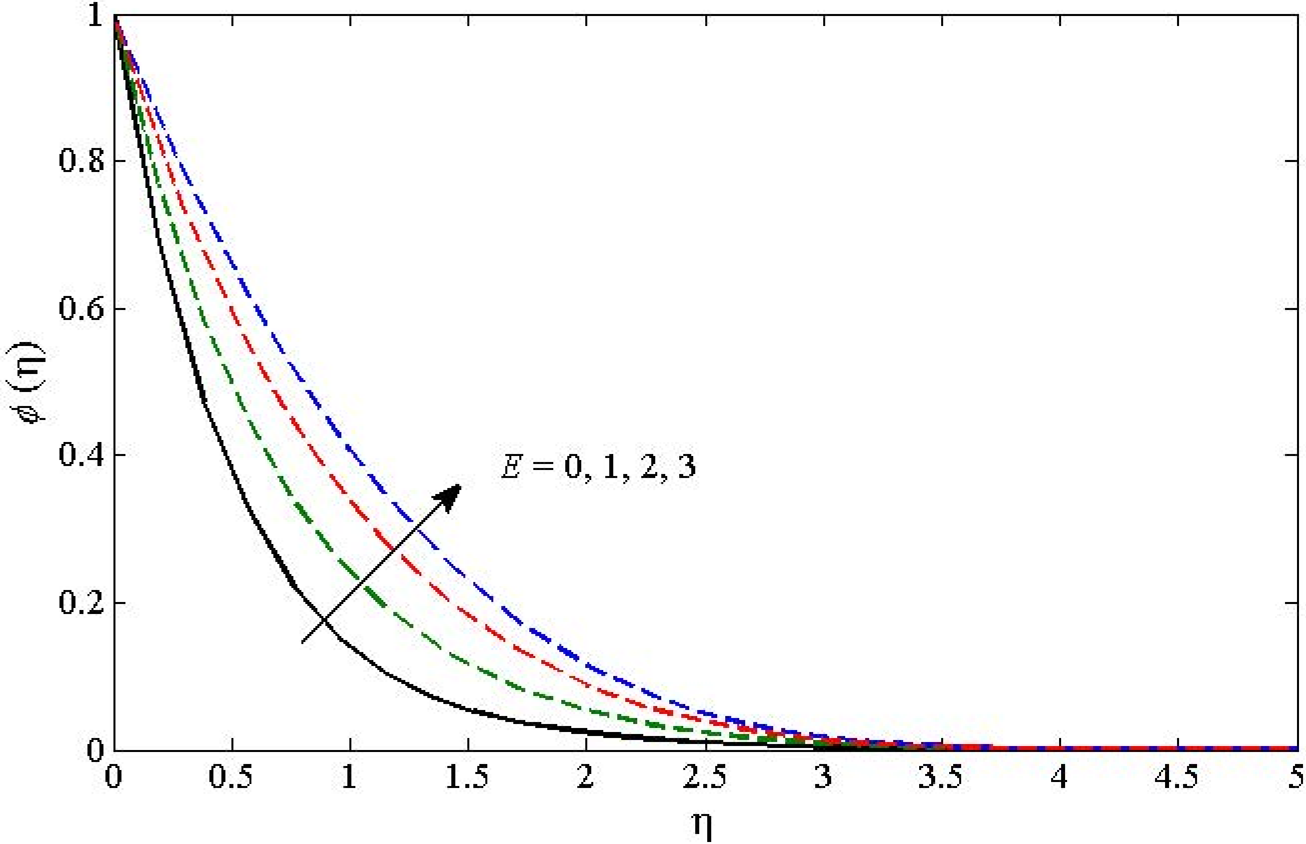

1
0.8
0.6
0.4
0.2
0
φ (η)
E = 0, 1, 2, 3
0
0.5
1
1.5
2
2.5
3
3.5
4
4.5
5
η

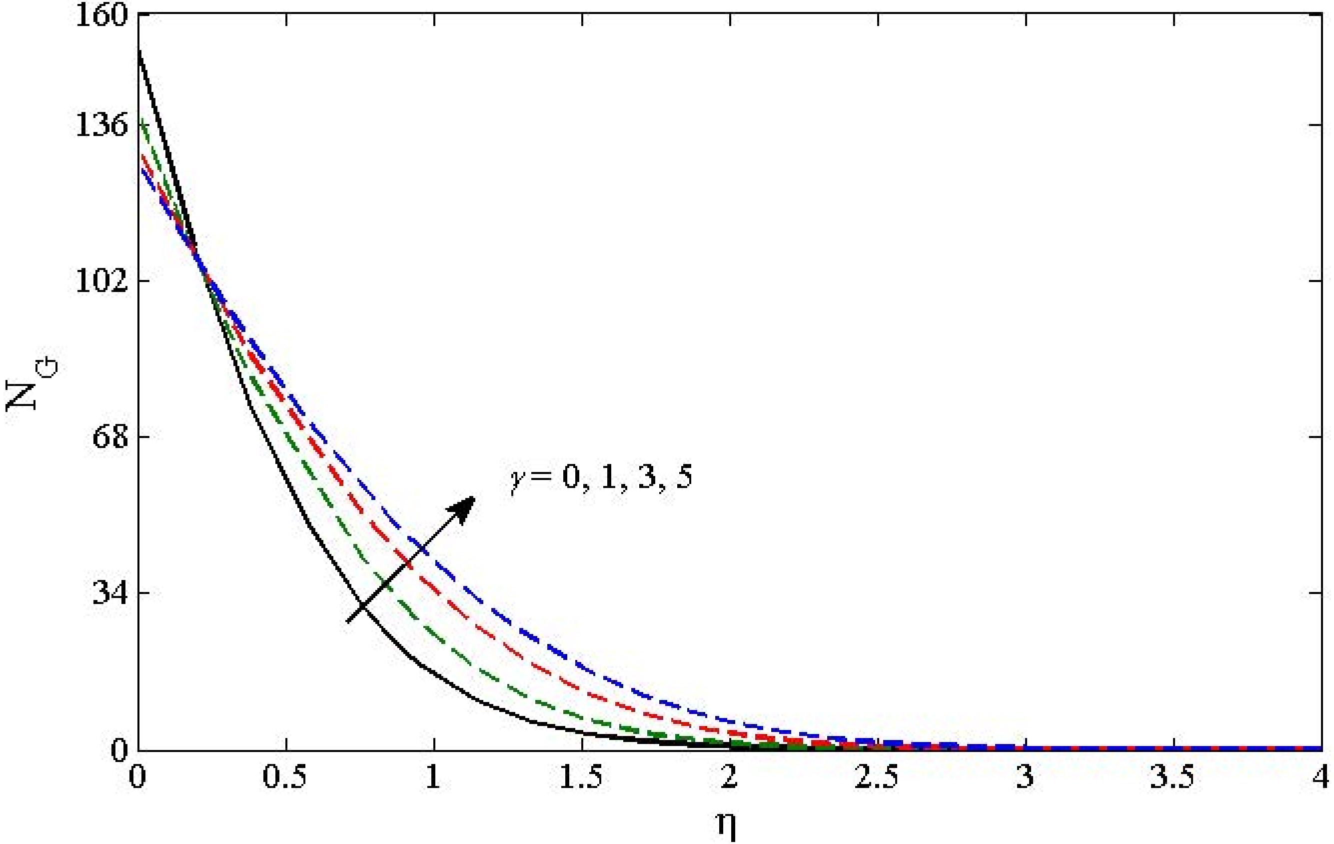
160
136
102
68
34
0
N_G
γ = 0, 1, 3, 5
0
0.5
1
1.5
2
2.5
3
3.5
4
η

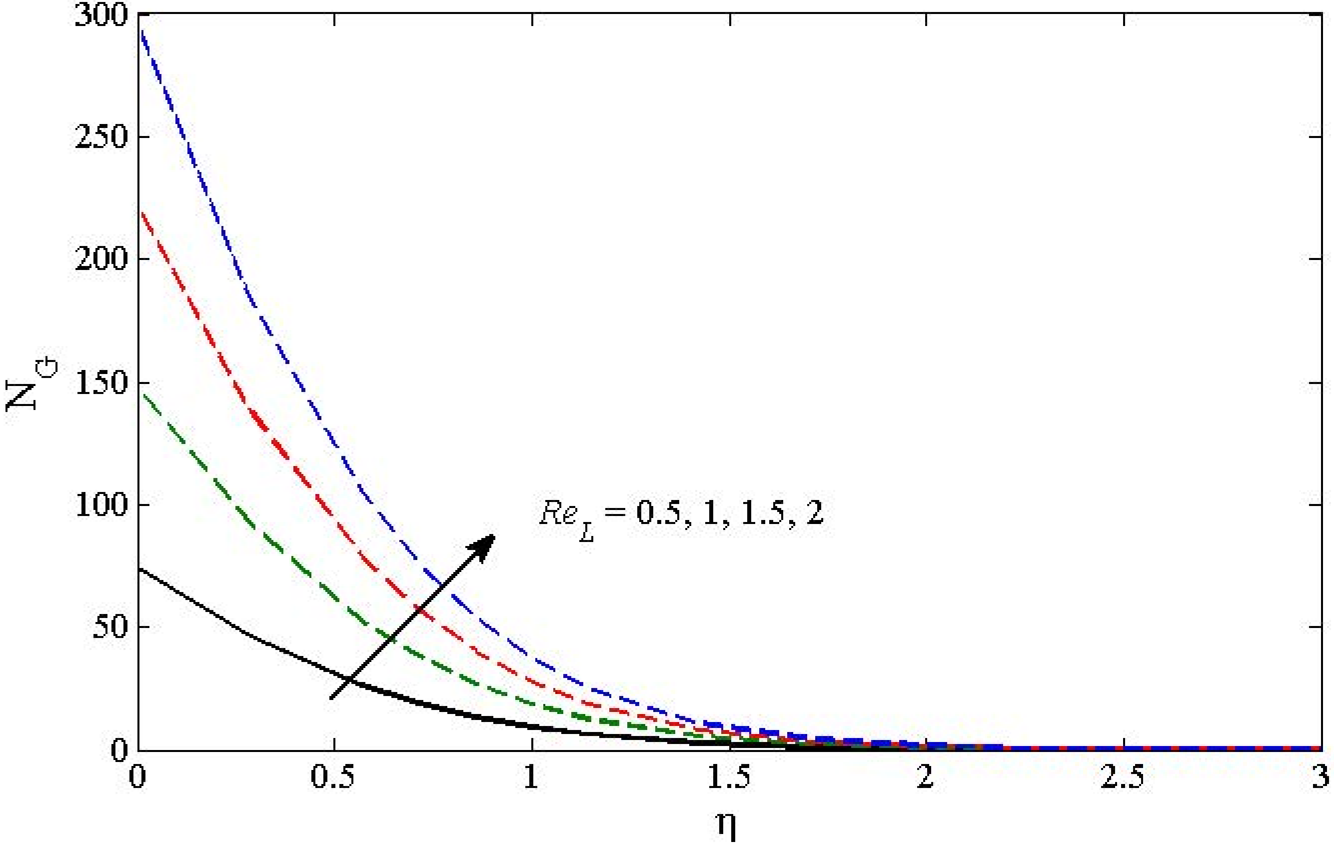

300
250
200
150
100
50
0
0
0.5
1
1.5
2
2.5
3
N_G
η
Re_L = 0.5, 1, 1.5, 2

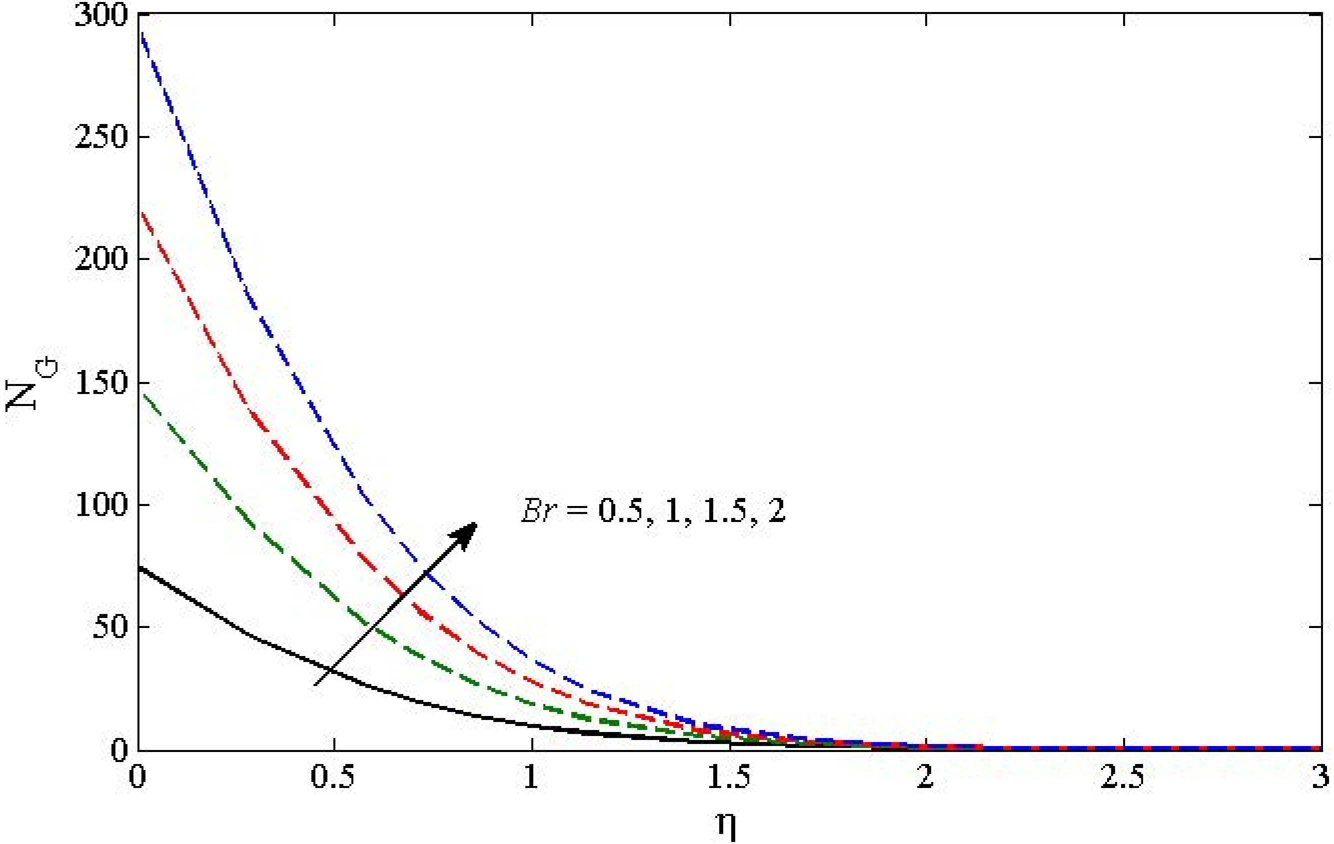

300
250
200
150
100
50
0
0
0.5
1
1.5
2
2.5
3
N_G
η
Br = 0.5, 1, 1.5, 2

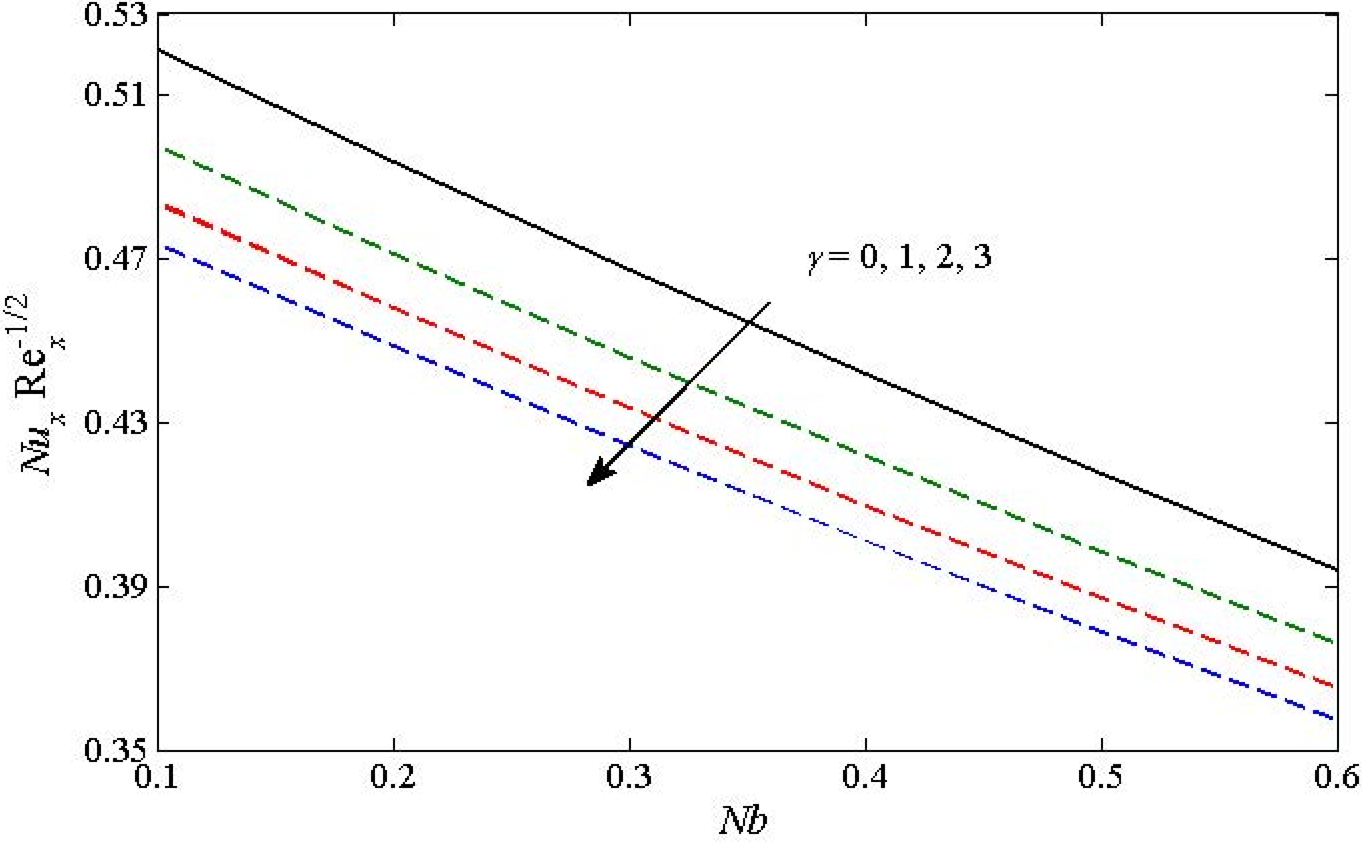
0.53
0.51
0.47
0.43
0.39
0.35
0.1
0.2
0.3
0.4
0.5
0.6
$Nu_x \, Re_x^{-1/2}$
Nb
$\gamma = 0, 1, 2, 3$

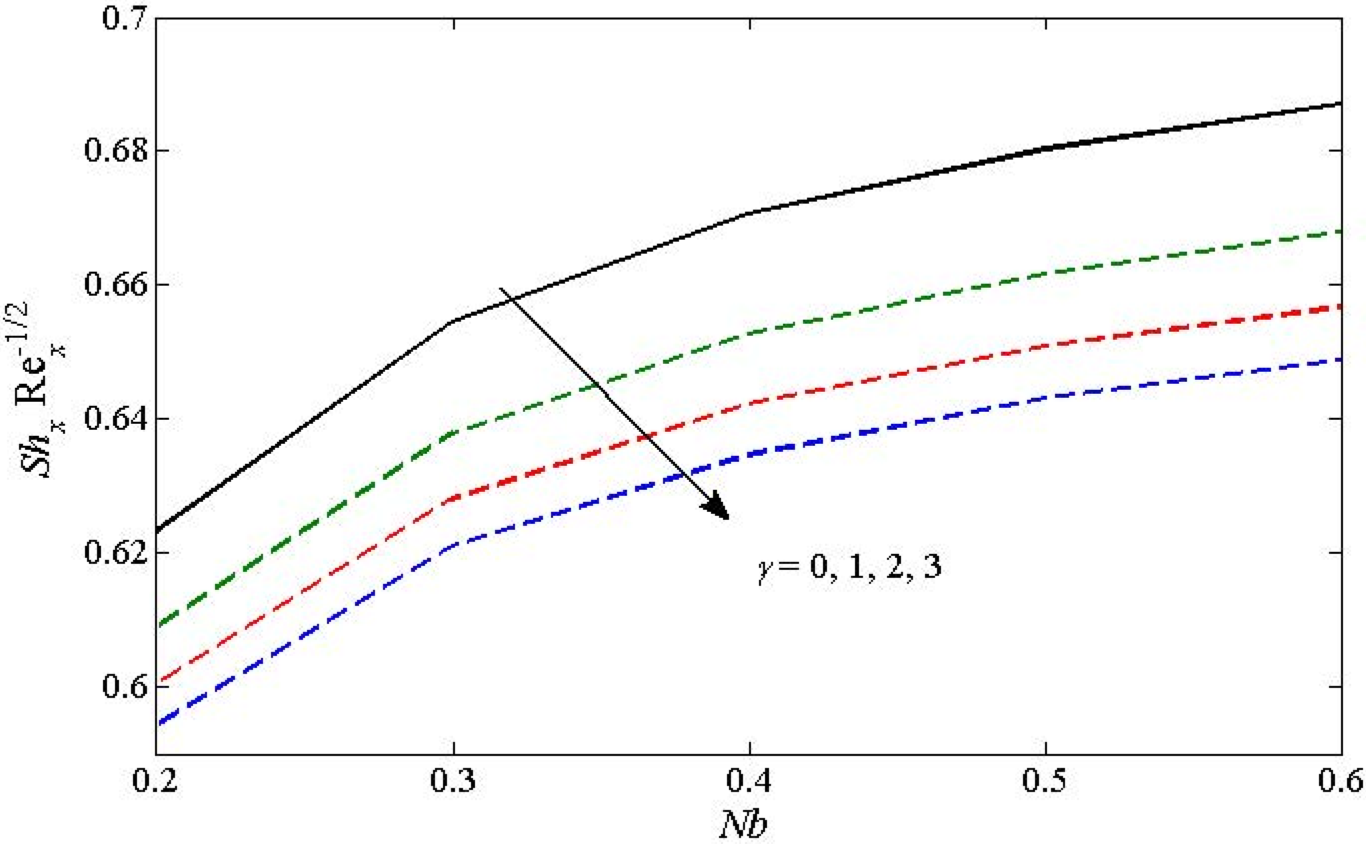

0.7
0.68
0.66
0.64
0.62
0.6
$Sh_x \, \mathrm{Re}_x^{-1/2}$
$\gamma = 0, 1, 2, 3$
0.2
0.3
0.4
0.5
0.6
Nb

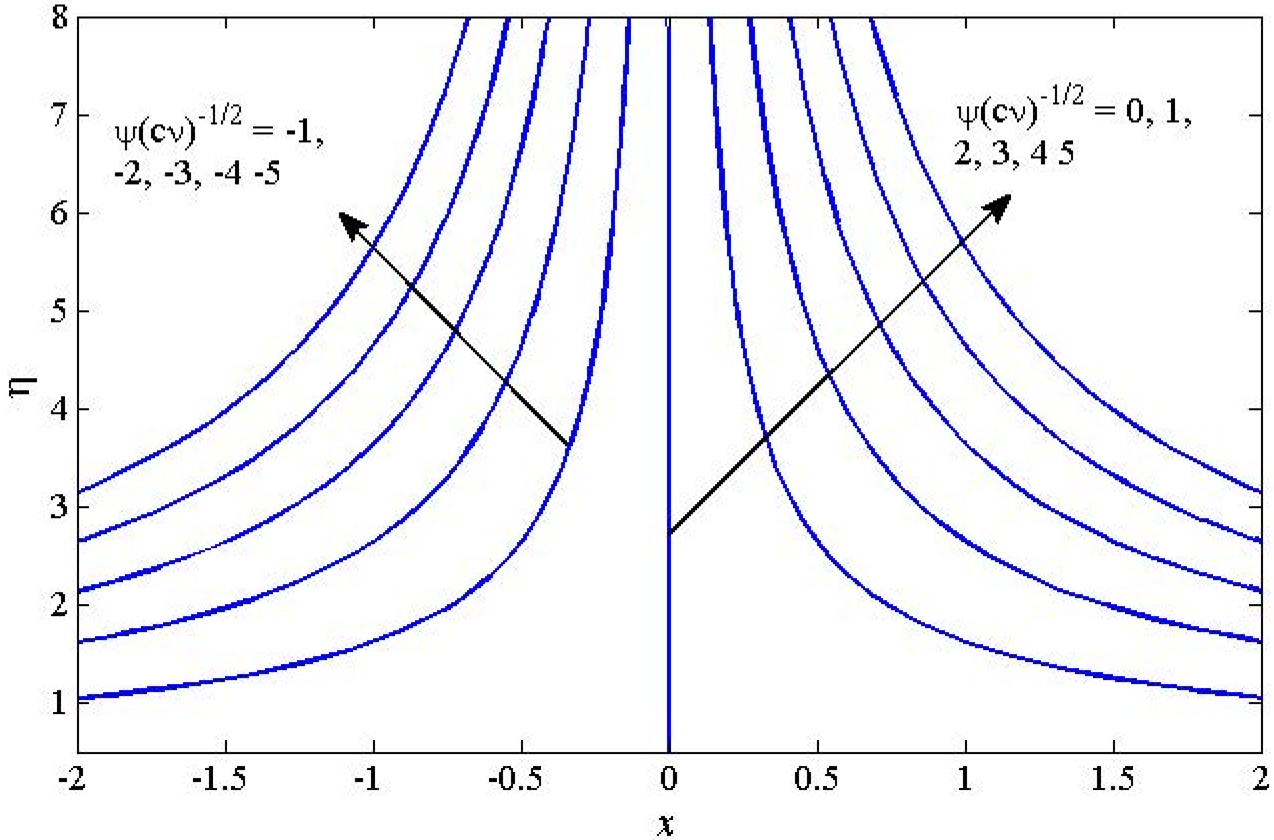

ψ(cν)^-1/2 = -1, -2, -3, -4 -5
ψ(cν)^-1/2 = 0, 1, 2, 3, 4 5
η
x
8
7
6
5
4
3
2
1
-2
-1.5
-1
-0.5
0
0.5
1
1.5
2